

Development of a Support-Vector-Machine-based
Supervised Learning Algorithm for Land Cover Classification
using Polarimetric SAR Imagery

James Noel Black

Thesis submitted to the faculty of the Virginia Polytechnic Institute and State University in
partial fulfillment of the requirements for the degree of

Master of Science
In
Electrical Engineering

Lamine M. Mili, Chair
Ahmed Abdelhadi
Amir I. Zaghloul

August 30, 2018
Falls Church, VA

Keywords: Synthetic Aperture Radar, Support Vector Machine, Robust, Polarimetric

Development of a Support-Vector-Machine-based Supervised Learning Algorithm for Land Cover Classification using Polarimetric SAR Imagery

James Noel Black

ABSTRACT

Land cover classification using Synthetic Aperture Radar (SAR) data has been a topic of great interest in recent literature. Food commodities output prediction through crop identification, environmental monitoring, and forest regrowth tracking are some of the many problems that can be aided by land cover classification methods. The need for fast and automated classification methods is apparent in a variety of applications involving vast amounts of SAR data. One fundamental step in any supervised learning classification algorithm is the selection and/or extraction of features present in the dataset to be used for class discrimination. A popular method that has been proposed for feature extraction from polarimetric data is to decompose the data into the underlying scattering mechanisms. In this research, the Freeman and Durden scattering model is applied to ALOS PALSAR fully polarimetric data for feature extraction. Efficient methods for solving the complex system of equations present in the scattering model are developed and compared. Using the features from the Freeman and Durden work, the classification capability of the model is assessed on amazon rainforest land cover types using a supervised Support Vector Machine (SVM) classification algorithm. The quantity of land cover types that can be discriminated using the model is also determined. Additionally, the performance of the median as a robust estimator in noisy environments for multi-pixel windowing is also characterized.

Development of a Support-Vector-Machine-based Supervised Learning Algorithm for Land Cover Classification using Polarimetric SAR Imagery

James Noel Black

GENERAL AUDIENCE ABSTRACT

Land type classification using Radar data has been a topic of great interest in recent literature. Food commodities output prediction through crop identification, environmental monitoring, and forest regrowth tracking are some of the many problems that can be aided by land cover classification methods. The need for fast and automated classification methods is apparent in a variety of applications involving vast amounts of Radar data. One fundamental step in any classification algorithm is the selection and/or extraction of discriminating features present in the dataset to be used for class discrimination. A popular method that has been proposed for feature extraction from polarized Radar data is to decompose the data into the underlying scatter components. In this research, a scattering model is applied to real world data for feature extraction. Efficient methods for solving the complex system of equations present in the scattering model are developed and compared. Using the features from the scattering model, the classification capability of the model is assessed on amazon rainforest land types using a Support Vector Machine (SVM) classification algorithm. The quantity of land cover types that can be discriminated using the model is also determined and compared using different estimators.

Acknowledgments

I would like to convey my sincerest gratitude to those who guided and supported me through the completion of this work. Firstly, I thank Dr. Mili who, throughout my coursework and research, always pushed me to give my very best and tirelessly listened, guided, and inspired my research. I thank Dr. Zaghloul and Dr. Abdelhadi for their willingness to serve on my committee and provide feedback. I also thank Justin Fishbone for his encouragement and advice. Lastly, I thank my family for their unwavering support through it all and without whom this thesis would not have been possible.

Table of Contents

Acknowledgements.....	iv
Table of Contents.....	v
List of Figures.....	vii
List of Tables.....	viii
List of Acronyms.....	ix
Chapter 1 - Introduction.....	1
1.1) Background.....	1
1.1.1) Synthetic Aperture Radar Description.....	2
1.1.2) Current Radar Image Classification Methods.....	4
1.2) Current Method Shortfalls.....	5
1.3) Contributions.....	6
1.4) Thesis Outline.....	6
Chapter 2 - Literature Review of Supervised Learning.....	8
2.1) Feature Extraction.....	8
2.2) Classification methods.....	10
Chapter 3 - Proposed Method Description.....	13

3.1) Freeman-Durden Description.....	13
3.2) Freeman-Durden Solution.....	14
3.3) Window Size and Median Estimation.....	17
3.4) SVM Description.....	18
3.5) SVM Kernel Function.....	20
3.6) Cross-validation.....	21
Chapter 4 - Application Description	22
4.1) Problem Formulation.....	22
4.2) Raw-data Preprocessing Description.....	23
Chapter 5 - Experimental Results.....	25
Chapter 6 - Conclusions and Future Work.....	33
6.1) Conclusions.....	33
6.2) Future Work.....	34
References.....	37
Appendix A - Implementation of Proposed Model in Matlab.....	40

List of Figures

- 4.1 Terraclass Project Land cover classifications used as ground truth for this research
- 4.2 Advanced Land Observing Satellite fully polarimetric Synthetic Aperture Radar image ground footprint used for classification studies in this thesis (courtesy of the Alaska Satellite Facility).
- 5.3 Raw SAR complex data on the left and the classification results of the same image on the right for the three-class problem
- 5.4 Training data sites for the Support Vector Machine classifier
- 5.5 Two-class classification problem results
- 5.6 Three-class classification problem results
- 5.7 Four-class classification problem results
- 5.8 Four-class results using the median estimator in windowing as opposed to the ensemble average
- 5.9 Training areas for two-class forest type classification problem
- 5.10 Left figure is the results of the two-class forest types classification and the figure on the right is the raw SAR image

List of Tables

Table 5.1 Classification results by pixel percentage for all SVM models

List of Acronyms

ALOS	Advanced Land Observing Satellite
CNN	Convolutional Neural Network
MLC	Maximum Likelihood Classifier
PDF	Probability Density Function
POLSAR	Polarimetric Synthetic Aperture Radar
PRF	Pulse Repetition Frequency
RBF	Radial Basis Function
SAR	Synthetic Aperture Radar
SVM	Support Vector Machine

Chapter 1

Introduction

1.1) Background

Rainforest deforestation quantification and crop type identification are a few applications that can benefit from efficient Synthetic Aperture Radar (SAR) classification methods.

Increasingly, airborne and space-borne sensors such as the Advanced Land Observing Satellite (ALOS) equipped with fully polarimetric SAR sensors are being fielded. The advantage of fully polarimetric data is that it adds the dimension of electromagnetic field orientation in the return data which can be used to improve overall classification capability. Different surface scattering features are manifested in unique polarimetric responses that can be exploited for classification purposes. Furthermore, the L-band Polarimetric SAR sensor on ALOS has been shown in recent studies to be ideal for rain forest land cover differentiation [1].

Historically, many feature extraction algorithms for SAR classification have been purely mathematical in nature without a true basis in physical models. For example, Cloude and Pottier

proposed a decomposition into three orthogonal components which may be too restrictive for a true physical model [3]. The Cloude and Pottier model is based in eigenvalue analysis and employs a statistic known as scattering entropy. More recently, however, physical model based polarimetric SAR decompositions have been proposed. Freeman and Durden have developed a three-component scattering model that is rooted in distinct physical scattering mechanisms. The three mechanisms represent canopy/volume scatter, surface scatter and double bounce scatter. Additionally, a four-component physical model has been proposed by Yamaguchi to extend the Freeman and Durden model to include a fourth helical scattering component [6].

1.1.1) Synthetic Aperture Radar Description

Synthetic Aperture Radar is a type of imaging radar in which the movement of the antenna platform over an interval of time produces a much larger effective antenna size, thus increasing the radar's azimuthal resolution. In fact, the azimuthal resolution is inversely proportional to the platform velocity of the SAR system [5]. Due to the platform velocity that is necessary for fine resolutions, these radar platforms are typically airborne or spaceborne. To generate an image, the system integrates chirp pulses sent at a certain pulse repetition frequency (PRF) over a coherent interval of time. This period of time corresponds to the SAR aperture length and is inversely proportional to the azimuth resolution [12]. So, as the coherent interval is increased for a SAR sensor at the same velocity, the azimuthal resolution becomes finer. Additionally, the real aperture length of the physical sensor at a constant velocity is exactly twice the azimuthal resolution [10]. In other words, a very small SAR antenna can theoretically

produce very fine azimuthal resolutions. The other dimension for resolution in a SAR system, range resolution, is determined by the inverse of the Radar bandwidth.

Unlike optical sensors, radar sensors are not sensitive to cloud cover and they can provide both amplitude and phase information. Additionally, polarimetric SAR sensors also provide the added feature of polarization orientation. It has been shown that L-band is the optimal frequency for land cover classification [7]. Although fully polarimetric L-band platforms such as ALOS PALSAR have been collecting data for some time now, very few studies into the rain forest classification ability have been carried out [1].

SAR image processing suffers from a phenomenon known as speckle noise. This is a type of multiplicative noise where the amplitude of the return in a resolution cell follows a Rayleigh distribution given by the probability density function (PDF) [10]:

$$p(A|\sigma^2) = \frac{2A}{\sigma^2} \exp\left(\frac{-A^2}{\sigma^2}\right), A \geq 0 \quad (1)$$

Where A is the amplitude, and σ^2 is the variance. Speckle noise can be viewed as a trade between contrast and variance since the variance must be decreased to increase the contrast [10]. The noise can be effectively mitigated by taking multiple looks of the same area and averaging the results to reduce the variance. Another method that is often used is to create a window that contains the average of a few pixels. This technique reduces variance at the expense of resolution.

Another issue that arises in SAR imaging are distortions in the image projection onto the ground. Typically, a SAR sensor is not generally located overhead of the image area, but rather is viewing the ground at an angle θ . Due to the ground topography and the θ view angle, various distortion effects occur in the image. The two-dimensional projection of the returned energy can be described by [10]:

$$E(x, R) = \int (x, y_0 + R \sin \theta, z_0 - R \cos \theta) R d\theta \quad (2)$$

Where R is the range, E is the energy received, and x,y,and z are the cartesian coordinates of the 3D ground topography. It is important to notice that a specific point in the 2D receive plane is an integral over the angle θ . Therefore, the energy returned from the top of a sharp mountain will be overlaid onto the valley before it if the two points have the same range to the SAR receiver. Additionally, at a sharp angle θ , that same mountain will obscure the far side of the mountain since it will be in the Radar shadow. Lastly, the effect of foreshortening is related to layover but where the base of the mountain is actually closer to the receiver than the top causing the mountain slope to be compressed in the image. All three of these phenomena can cause significant distortions in the ground-plane projected image, depending on the roughness of the terrain and severity of the look angle θ . These distortions need to be taken into account when the imagery is interpreted and classified in the results to follow.

1.1.2) Current Radar Image Classification Methods

In the Amazon, rainforest land cover type classification is an important issue. The area is home to some of the world's most biodiversity yet is also the subject of human caused deforestation. Classification algorithms that can be run on vast amounts of Amazon rainforest area can assist in auditing deforestation for compliance with laws and regulations. In addition, classification methods may be able to characterize the regrowth of the forests over time [1].

There are many machine learning methods that have been successfully applied to Radar image classification problems. This include supervised methods such as Maximum Likelihood Classifier (MLC) and Support Vector Machine (SVM) as well as unsupervised clustering

methods such as K-means. MLC is a probabilistic method that relies on the statistical representation of each of the classes. In Radar image applications, the Wishart distribution is the most appropriate. Once the class distribution models are created, the classifier works by calculating the probability that each data point is from each class and choosing the class with the highest probability [1]. The SVM technique works to optimally separate two classes with a hyperplane in the feature space and is independent of data distribution and is robust with respect to the Hughes phenomenon [2]. The Hughes phenomenon first demonstrated in 1968, showed that for a given sample data size, increasing the feature dimensionality leads to maximum classification accuracy and then decreases thereafter for a Bayesian classifier.

1.2) Current Method Shortfalls

Many of the current methods used for feature extraction in polarimetric SAR image classification lack a physical model. For example, the popular alpha-entropy decomposition does not account for distinct scattering mechanisms that are distinguishable with polarimetric data. As a result, the classification results are inherently diminished without exploiting the information contained in the scattering mechanisms. Physics based models that rely on scattering mechanisms such as the Freeman-Durden and Yamaguchi have largely not been used in image classification investigations.

Some modern machine learning algorithms such as the Convolutional Neural Network (CNN) do not rely on advanced feature extraction methods. Instead, the raw complex SAR data can be fed directly into the CNN classifier, skipping the traditional feature extraction step. While this method can be beneficial and has been successfully applied to many applications

including image classification, there are drawbacks. CNN for image classification requires vast amounts of training data to ensure good performance. Due to the high cost of fielding airborne and spaceborne SAR platforms, image data can be quite limited. Also, CNN's are computationally expensive. With all the training data being fed into the model, computational complexity is high. Although CPU's and GPU's have been dropping significantly in price and increasing significantly in performance, computational complexity of algorithms still needs to be considered. Other supervised machine learning algorithms such as SVM rely on a good feature extraction model, but do not require vast amounts of training data and have lower computational complexity than CNN's.

1.3) Contributions

This thesis expands on the work of the Freeman and Durden paper. The equations presented in the paper for feature extraction are solved explicitly and implemented in Matlab on real SAR datasets in this research. The Freeman and Durden feature extraction method is combined with a one-vs-one multiclass SVM to characterize the performance of land cover type discrimination specifically in the Amazon rainforest region. A robust windowing technique utilizing the median estimator is used to improve the performance of the classifier in speckle noisy environments. The resulting performance of the classification method is compared to previous studies such as Negri et al.

1.4) Thesis outline

An extensive literature review is presented in chapter 2. The review explores both current feature extraction methods as well as supervised learning algorithms that have been applied specifically to polarimetric SAR image classification. Additionally, the performance of these methods to current land cover classification problems such as crop identification and rain forest regrowth characterization is investigated. Chapter 3 contains a detailed description of the physics-based classification model. Chapter 4 describes the specific rainforest classification application for model testing and then chapter 5 presents the results of the study. Chapter 6 contains the conclusions that came out of the study and recommendations for future work.

Chapter 2

Literature Review of Supervised Learning

1.1) Feature Extraction

In the study of Polarimetric SAR, much emphasis has been placed on determining the underlying scattering mechanisms present in the backscatter return of various surface features. The importance of characterizing these mechanisms is fundamental to the ability to classify land cover types. If certain land cover types exhibit certain scattering mechanisms, that information can be exploited for efficient land cover classification. Freeman and Durden describe a method to decompose SAR complex data into three scattering mechanisms, namely volume, surface and double-bounce. Chen corroborates that these are the main three scattering mechanisms present in SAR [10]. However, later on Chen modifies this model to include five distinct scattering mechanisms that are rough surface, low-order multiple scattering, random volume scatter, surface scatter, and single scatter from anisotropic structures. These five scattering mechanisms were introduced by Cloude in his explanation of target decomposition [11].

In addition to the Freeman-Durden model, the Cloude and Pottier decomposition model introduced in 1997 is also commonly used to decompose the polarimetric scattering matrix [3]. This method is an eigenvector decomposition which produces three parameters namely, entropy, alpha angle, and anisotropy. The Cloude and Pottier method is capable of identifying the three primary scattering mechanisms of volume, surface and backscatter as zones in a 2D plot of alpha and entropy. While this is not as direct of a physical model for the scattering mechanisms as the Freeman and Durden method, it has still been shown to produce good results. The Cloud-Pottier method, also known as alpha-entropy, is typically used to identify volume vs rough surface scatter. The anisotropy parameter determines the dominance level of a single scattering mechanism. If the anisotropy is low, multiple secondary scattering mechanisms are present, and if the anisotropy value is near one, one of the secondary scattering mechanisms is dominant [13].

The journal article by Adams et al evaluated the discrimination capability of C-band Polarimetric SAR data for determining unharvested crops vs post-harvest crops using the alpha-entropy method and the Freeman and Durden method. The conclusion of the study determined that there was general agreement in the two methods for determining the harvested vs. unharvested fields. The authors do suggest that there is likely more utility in in these decompositions in determining land cover classification types instead of the temporal classification of pre-harvest and post-harvest. Though this study concluded with the similar utility of the two decompositions it should be noted that this was with C-band data used for temporal classification, verses the L-band data used in this research for land cover classification types.

2.2) Classification methods

Given the high level of interest in land cover classification, many types of classification techniques have been employed in recent literature with the goal of achieving the best results possible. The types of techniques can generally be placed into a few distinct categories. There are feature-based methods which use the parameters produced by models such as the Freeman and Durden or alpha entropy to train a classifier such as SVM or neural network. Alternatively, there is the Bayesian maximum likelihood method in which the probability density function for each class is estimated from the training data. Classification on samples is performed by determining the statistical likelihood that a sample came from each of the classes and then choosing the class that has the maximum likelihood. The first challenge with this technique is finding an accurate distribution model with the parameters to be estimated. The most common distribution used in recent literature is the complex Wishart distribution. The reason is that for the common assumption of fully developed speckle, the polarimetric scattering matrix follows a Wishart distribution.

Many current studies have explored the capability of a support vector machine classifier as a feature-based method. One recent study evaluated the classification potential of SVM for forest classification using RadarSat-2 C-band Polarimetric SAR data [17]. While C-band has been shown to not be the ideal frequency for land cover classification, the potential was still explored.

Another recent study used the Wishart distribution model to develop a bayesian maximum likelihood classifier based on a distance metric [14]. Class determination was performed by choosing the class with the shortest distance between the average covariance

matrix of that class's Wishart distribution and the sample pixel covariance. The results of the study showed accuracies of as high as 86% for determining the growth stages of agricultural crops using PolSAR imagery generated from the C-band RADARSAT-2. The paper proposed using a wrapper feature selection method to reduce the large number of features considered in order to speed up the SVM training algorithm. The results of the study showed about a 10 percent increase in classification accuracy over the Wishart classifier.

In addition to the supervised feature-based methods and the supervised wishart classifier previously described, various unsupervised techniques have also been effectively applied to land cover classification. Oftentimes these unsupervised techniques are initialized with training sets obtained from supervised classification algorithms. For example, one study used Alpha-entropy to initially classify a PolSAR image and then that training data is fed into a Wishart-based classifier. In the unsupervised process, the classified results are used to iteratively retrain the Wishart classifier until the number of pixels changing classes reaches a low enough threshold [15]. The outcome of the study found that there was improved performance through the use of iteration, and also that after the initialization step the unsupervised method is automated.

Another study in unsupervised methods applied spectral clustering to PolSAR data by performing a pairwise distance measurement on pixels based on the Wishart distribution [16]. Grouping according to this method has significant benefits over the Wishart unsupervised classifier. The major benefit is the ability for the pairwise distance algorithm to capture more complex clustering structures in the feature space. The method works by first computing the pairwise distances between all of the pixel's coherency matrices and transforming those to affinities by way of a Gaussian kernel function. Clustering is then performed in the eigenspace decomposition of the affinity matrix. Assuming the classes are separable, the clusters should

form around the orthogonal axes after algorithm iteration. One drawback of this method is its high computational complexity. The authors perform random sampling on the pixel data in order to significantly reduce the number of pixels for which pairwise distances and iterative classifications must be computed.

Chapter 3

Proposed Method Description

3.1) Freeman-Durden Description

The Freeman-Durden model is a polarimetric decomposition algorithm rooted in the physical scattering mechanisms present in natural environments. Three distinct scattering types are represented by the model. The first component is volume scatter commonly found in canopy backscatter where the energy is scattered uniformly in all directions. In the model, this phenomenon is represented by thin cylindrical scatterers exhibiting random orientation in 3D space. The second scattering component is double-bounce scatter. This type of scattering is found in natural environments anywhere there are right angles of two surfaces with different dielectric constants. One simple example of this would be the double bounce off the ground and a tree. For the purposes of the model, double bounce scatterers are assumed to be dihedral corner reflectors where the two surfaces have different dielectric constants. The final type of scatter is called surface scatter and is modeled as a Bragg surface from a rough surface.

Assuming that these three scattering components are mutually uncorrelated, a system of equations can be constructed with the relative contribution of each scattering component as the variable to be solved for.

3.2) Freeman-Durden Solution

The Freeman and Durden model for polarimetric decomposition culminates in three equations and four unknowns:

$$[|S_{hh}|^2] = f_s |\beta|^2 + f_d |\alpha|^2 \quad (3)$$

$$[|S_{vv}|^2] = f_s + f_d \quad (4)$$

$$[S_{hh}S_{vv}^*] = f_s \beta + f_d \alpha \quad (5)$$

The S quantities in equations 3-5 represent the scattering matrix complex values and the subscripts of S represent the transmit and received polarizations. For example, S_{hh} represents the received return from horizontal transmit and vertical receive. These are the “known” quantities in that they are estimated from the raw data. It should be noted that the square brackets on the left-hand side of the equations represent expected values such that those quantities are described probabilistically. Everything on the right-hand side of equations 3-5 are variables to be solved for. f_s and f_d are the surface and double bounce scatter variables, respectively. α and β are variables that arise from the double bounce scatter model and the Bragg surface scatter model, respectively. This system of equations becomes a solvable three equations in three unknowns

once an assumption is applied to fix either alpha or beta in the above equations. The assumption used in the Freeman and Durden model is that if the real part of the left-hand side of the third equation is positive that surface scatter is considered dominant and alpha is fixed be negative one. Otherwise double-bounce scatter is dominant, and alpha remains a variable while beta is fixed to be one. Solving this system of non-linear, complex equations efficiently is a critical step in the method, since this set of equations has to be solved for each pixel or window of a few pixels. To this end, several candidate solution methods were explored and compared. Gradient descent and Newton's method employ iterative techniques but if multiple solutions exist, the initial conditions will affect the solution that is reached by the algorithms. However, using substitution the above system of equations can be solved explicitly for the two cases:

Case 1 $real(S_{hh}S_{vv}^*) > 0$:

$$\alpha = -1$$

$$C_1\beta^2 + C_2\beta + C_3 = 0, \text{ where}$$

$$C_1 = [S_{hh}S_{vv}^*] - [|S_{vv}|^2] * \alpha$$

$$C_2 = [|S_{vv}|^2] * |\alpha|^2 - [|S_{hh}|^2]$$

$$C_3 = -[S_{hh}S_{vv}^*] * |\alpha|^2 + [|S_{hh}|^2]\alpha$$

Applying the quadratic formula to find β :

$$\beta = \frac{-C_2 \pm \sqrt{C_2^2 + 4 * C_1 * C_3}}{2 * C_1} \quad (6)$$

The other two variables can easily be found from β :

$$f_s = \frac{[S_{hh}S_{vv}^*] - [S_{vv}|^2] * \alpha}{\beta - \alpha} \quad (7)$$

$$f_d = [|S_{vv}|^2] - f_s \quad (8)$$

Case 2 $real(S_{hh}S_{vv}^*) < 0$:

$$\beta = 1$$

$$C_1\beta^2 + C_2\beta + C_3 = 0, \text{ where}$$

$$C_1 = [|S_{vv}|^2] * \beta - [S_{hh}S_{vv}^*]$$

$$C_2 = [|S_{vv}|^2] * |\beta|^2 + [|S_{hh}|^2]$$

$$C_3 = [S_{hh}S_{vv}^*] * |\beta|^2 - [|S_{hh}|^2]\beta$$

Applying the quadratic formula to solve for α :

$$\alpha = \frac{-C_2 \pm \sqrt{C_2^2 + 4 * C_1 * C_3}}{2 * C_1} \quad (9)$$

The other two variables can easily be found from α :

$$f_s = \frac{[S_{hh}S_{vv}^*] - [S_{vv}]^2 * \alpha}{\beta - \alpha} \quad (10)$$

$$f_d = [|S_{vv}|^2] - f_s \quad (11)$$

Through an analysis of the solutions, it was found that only the positive quadratic solution results in a physically meaningful result. Once f_s and f_d are determined from the raw SAR complex data using equations 7-8 or 10-11, the relative powers of each of the three scattering mechanisms P_s , P_d , and P_v can be solved for using the equations [4]:

$$P = P_s + P_d + P_v = (|S_{HH}|^2 + 2|S_{HV}|^2 + |S_{vv}|^2) \quad (12)$$

$$P_s = f_s(1 + |\beta|^2) \quad (13)$$

$$P_d = f_d(1 + |\alpha|^2) \quad (14)$$

$$P_v = 8f_v/3 \quad (15)$$

Where P is the total power. The three powers, P_s , P_d , and P_v can then be used as the features fed into the SVM classification model.

3.3) Window size and median estimation

Windowing is a technique used to combine sample cells to help filter out speckle noise. This speckle noise is a multiplicative noise that normally results from the coherent sum of scatterer responses in a single pixel. For a Gaussian received signal amplitude distribution, this results in a rayleigh distribution in the pixel amplitude [5]. So even sample regions with the same mean Radar cross section can result in different pixel amplitudes. Averaging pixels over a window of 2x2 or 3x3 pixels has been shown to effectively mitigate speckle noise at the expense

of resolution. Other techniques used to reduce speckle noise include filtering and combining multiple looks of the same scene over time.

A 3x3 non-overlapping window was investigated both to help filter out speckle noise and reduce the time for the feature extraction step. The sample median of the cells in the window was also calculated instead of the mean to provide a robust estimate over the chosen window. The medians of the raw amplitude and phase data were set as the respective expected values for $[|S_{hh}|^2]$, $[|S_{vv}|^2]$, and $[S_{hh}S_{vv}^*]$.

3.4) SVM description

A Support Vector Machine (SVM) is used as a classification method to discriminate the various classes embedded in the raw data. For two-class data non-linearly mapped to a sufficiently high dimensional feature space, SVM's can guarantee that a hyperplane exists to separate the data [8]. A support vector machine seeks to find the optimal hyperplane separating the two classes such that the margin between the two classes is maximized. In the algorithm, only a subset of the data points closest to the class boundary are used in the calculation of the optimal hyperplane and these data points are known as support vectors.

In the two-class optimal hyperplane separation algorithm first introduced in 1995 by Cortes and Vapnik, assume that there exists a training data set \mathbf{x} in a high dimensional feature space with class labels \mathbf{y} of either 1 or -1 to describe the two classes [9]. Any hyperplane can be described in Hesse normal form by:

$$\mathbf{w} * \mathbf{x} + b = 0 \tag{16}$$

In order for the two classes to be linearly separable in feature space, the following inequality must be satisfied for all training data points for some distinct hyperplane determined by a fixed w and b :

$$y_k(\mathbf{w} * \mathbf{x}_i + b) \geq 1 \text{ for all } i \quad (17)$$

It can also be shown that the distance between the optimal hyperplane and a training data point is given by:

$$distance = \frac{2}{|w|} \quad (18)$$

Therefore, we have an optimization problem of minimizing w to maximize the distance between the training data points and the hyperplane, under the inequality constraint (equation 17). This optimization problem can be reformulated as a quadratic programming problem by transforming it into its lagrangian dual problem. It should be noted here that this solution only works if there is a so-called “hard margin” between the two classes, meaning that the feature space is linearly separable. A separate optimization problem and the more general solution for the “soft-margin” problem can also be formulated in cases where there is spillover in the class boundary.

SVM’s have certain advantages over other supervised classification techniques such as neural networks. For one, the computational complexity of the algorithm is related to the number of chosen support vectors and not the number of dimensions in the feature space [8]. Incidentally, this phenomenon has the added benefit of making SVM’s less susceptible to overfitting in the classification process than various other classification methods. One may think that since SVM’s can separate two classes in sufficiently high dimensional feature space and that

high dimensionality does not cost much in terms of computational complexity that higher dimensionality should always be chosen. Unfortunately, there exists a phenomenon known as the curse of dimensionality in which the sparsity of the data increases rapidly as the number of dimensions is increased. This has the effect of requiring an exponentially increasing number of data points as dimensionality is increased to provide any statistical discrimination in the data, especially if the problem is generalized to more than two classes.

Although SVM is fundamentally a pattern classification technique for only a two-class problem, there are schemes to extend the method for three or more classes. The most common and practical technique is to simply divide the multiclass problem into a series of two class problems. This can generally be achieved in one of two ways. In the one-vs-all method, n classifiers are created of each class vs all of the rest, where n is the number of classes. Final classification is determined by the SVM classifier that results in that data point having the maximum distance from a hyperplane and thus the highest confidence in the classification. In the one-vs-one approach, $n(n-1)/2$ SVM classifiers are created for all the possible two class combinations. Each data point is run through each of the classifiers and the class that has the most “votes” is determined to be the most likely final classification. For the purpose of this research, the one-vs-one approach was the implementation used.

3.5) SVM Kernel Function

The kernel function in a machine learning application is simply a similarity function which operates in a high dimensional feature space. The most basic kernel function that is used in SVM methods is the linear kernel function also known as the dot product. The linear kernel is

often preferred due to its mathematical simplicity and efficient computation. However, other kernel functions are common such as the quadratic kernel and the Radial Basis Function (RBF). RBF is the most general kernel function that is used when there is no prior information about the data. In this research, the linear kernel function was used for efficiency and simplicity.

3.6) Cross-Validation

Cross-validation is a statistical technique used to estimate the accuracy of a trained model by splitting the original training data into a training subset and a testing subset. The advantage is that by using part of the labeled original training set as a model testing set, one is able to test the accuracy of the model. This method is typically repeated many times with the training and testing data being rotated continuously such that a good estimate of the model accuracy is achieved. For every SVM trained in the results of this research, the model was cross-validated in MATLAB to ensure accuracy.

Chapter 4

Application Description

4.1) Problem Formulation

The objective of this study was to characterize the class discrimination capability of a SVM classifier applied to the Freeman and Durden model features extracted from raw polarimetric SAR complex data. More specifically, the discrimination capability of L-band polarimetric SAR in rainforest environments was sought to be determined. To achieve this, a large set of land cover classes were chosen and based on truth data. Then a small subset of those classes that were known to have high inherent discrimination likelihood in the Freeman and Durden model were run through the SVM classifier. Larger subsets were subsequently run through the classifier to determine at what point the model could no longer accurately classify the data. The truth dataset came from the TerraClass project 2010 data classification which provided detailed class labels for pieces of land cover corresponding to the test images. This truth dataset is in the form of shape files that can be overlaid on google earth imagery. Each

false color section represents a different classification type in the data. The test SAR images used from ALOS PALSAR were from 2010 also.

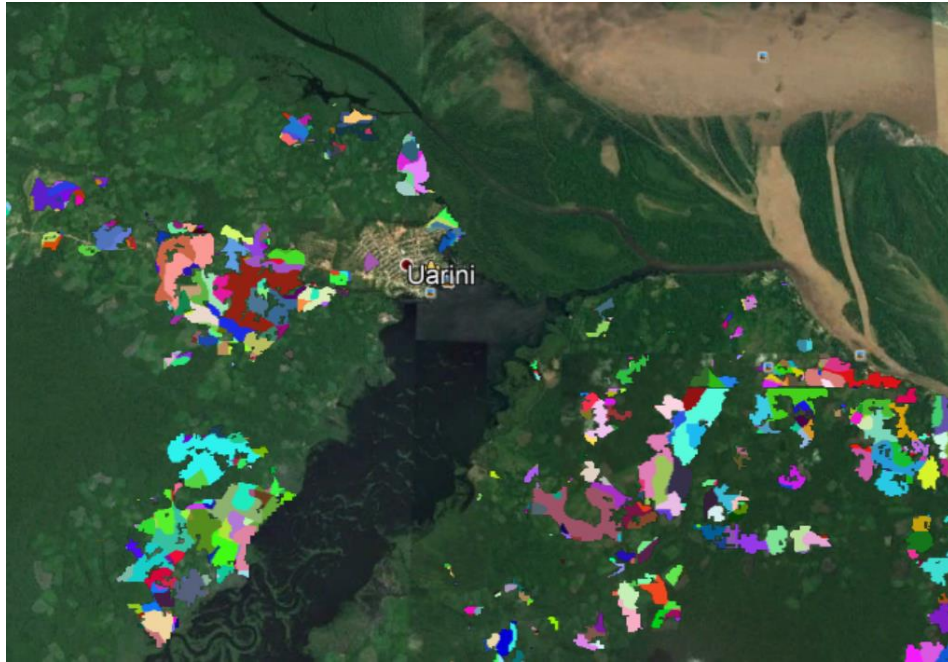


Figure 4.1: TerraClass project 2010 classification data overlaid on google earth imagery (data obtained from http://www.inpe.br/cra/projetos_pesquisas/terraclass2010)

4.2) Raw Data Preprocessing Explanation

The raw SAR data generated from ALOS PALSAR platform used in this study were obtained from the Alaska Satellite Facility with permission for use in educational purposes (Figure 4.2). The datasets were obtained as L1.1 raw complex data. The Alaska Satellite Facility MapReady version 3.1 software was used to process the raw data into four complex-

valued geotiff files representing each of the four polarization permutations. These are HH, HV, VH, and VV, where the first letter represents the transmit polarization either horizontal or vertical referenced to the ground and the second is the receive signal polarization also either vertical or horizontal. These four channels completely represent the polarimetric information contained in the radar response and collectively the dataset is therefore considered to be fully polarimetric.

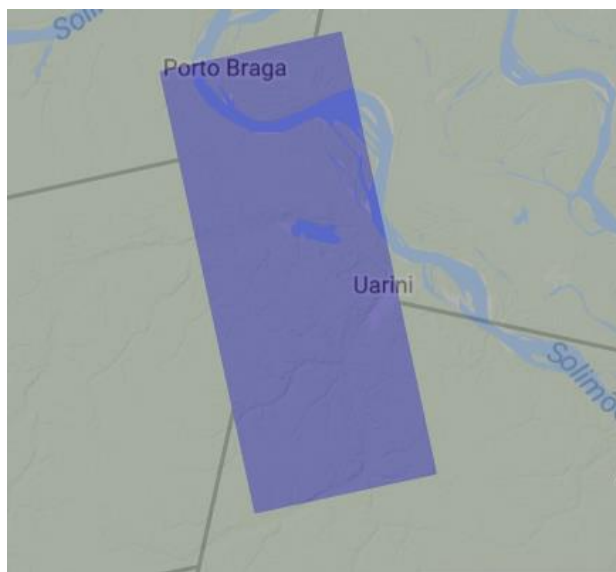


Figure 4.2: ALOS PALSAR fully polarimetric image ground footprint

Chapter 5

Experimental Results

The three-class case is shown in figure 5.3. The classes based on the truth data were water, farmland, and urban depicted as false color blue, green, and red, respectively. The SAR image on the right is 750 by 750 pixels. The Freeman and Durden feature extraction was performed on the mean of a 3 by 3 pixel window and the resulting feature space data was fed to the SVM classifier. The training data for each class for the SVM model was chosen from the same feature mapped data with only a 10 by 10 pixel training set for each class as shown in figure 5.4. The training data included a forest class as a fourth class. Classification was applied to the whole image using the same 3x3 non-overlapping window such that the final classified image was 250 by 250 pixels. Even with the resolution down sampling factor of 3, the SVM classifier was clearly able to discriminate small bodies of water and rivers from land.

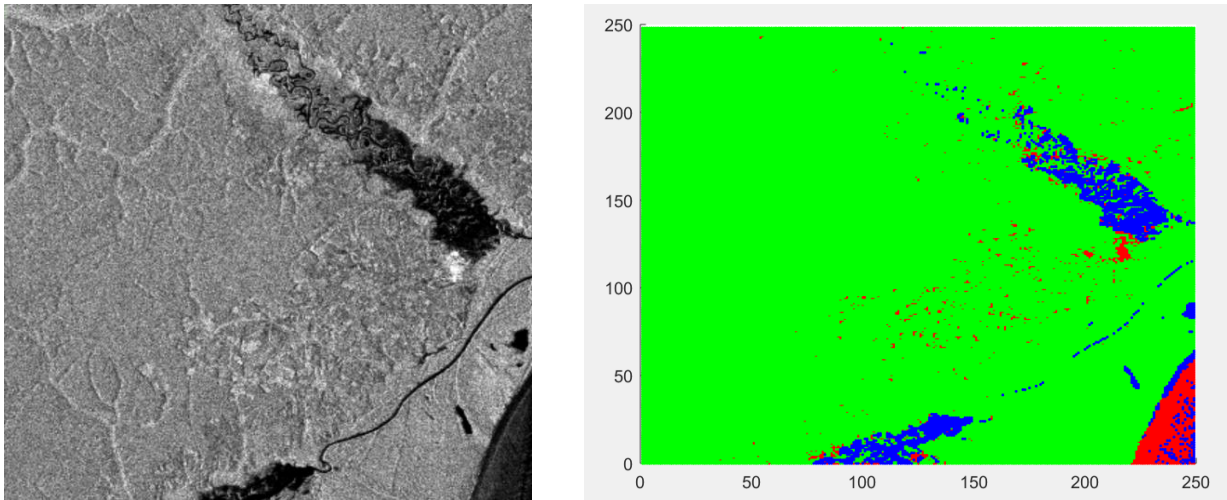


Figure 5.3: The left is the SAR image after raw complex preprocessing and the right image is the results of the SVM classifier.

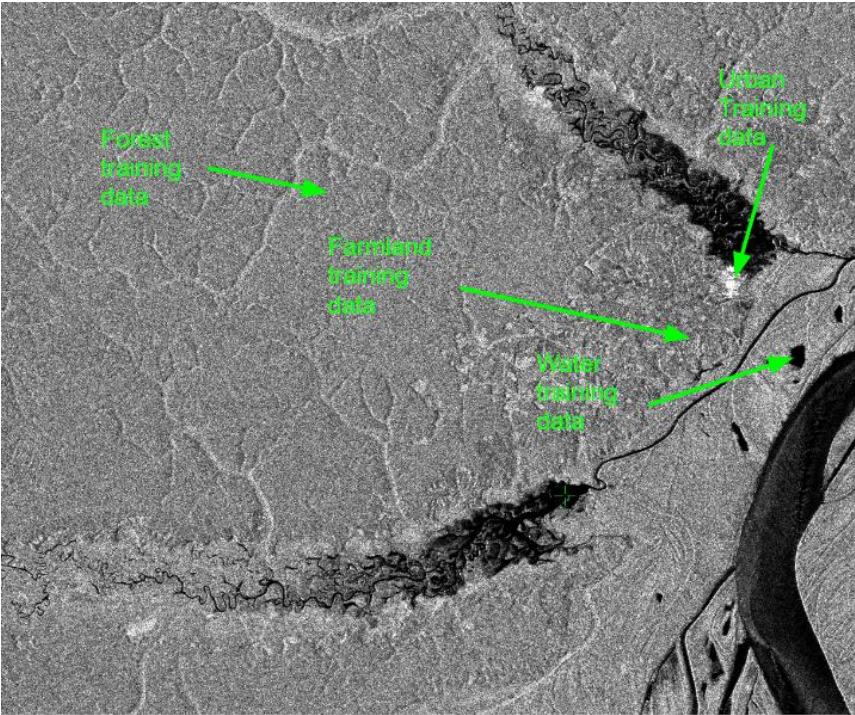


Figure 5.4: SVM training data sites

If only two of the three classes are considered, specifically the water class and the farmland class, the SVM classifier performs very well as shown in figure 5.5.

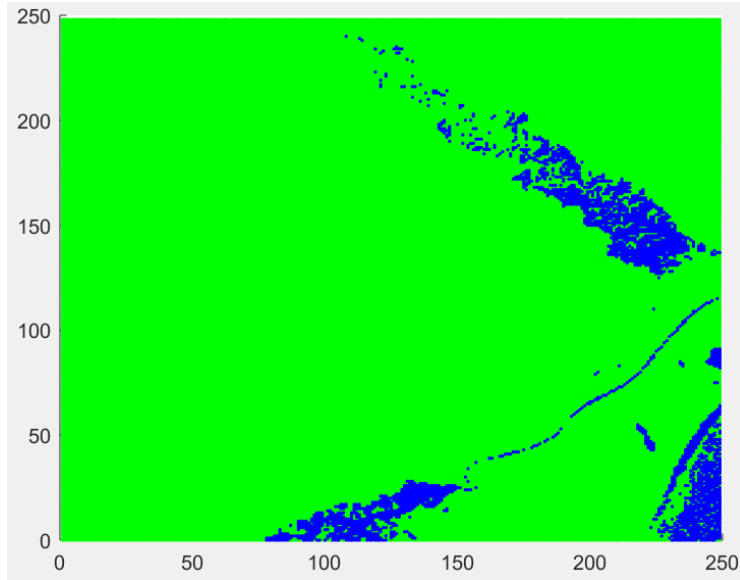


Figure 5.5: Two-class SVM classifier results for farm as green and blue for water

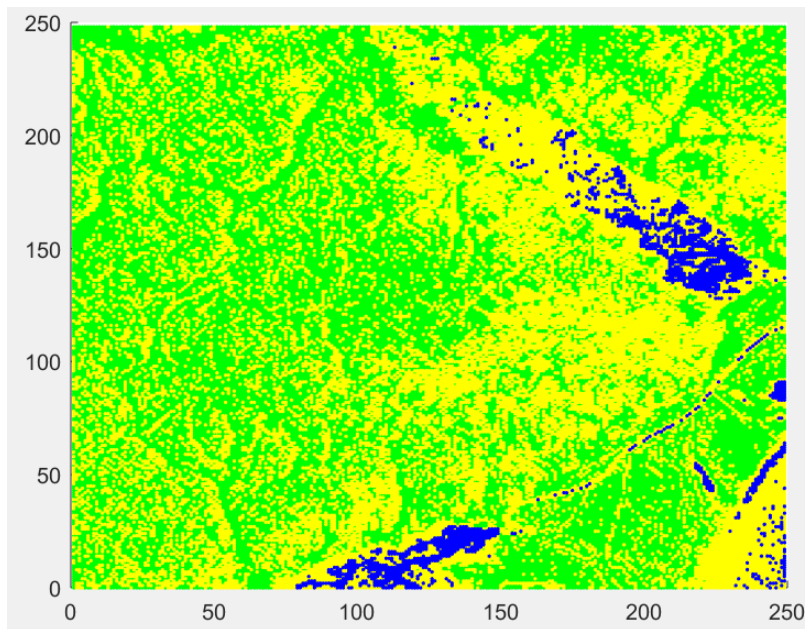


Figure 5.6: Three class SVM with blue as water, green as forest, and yellow as farmland.

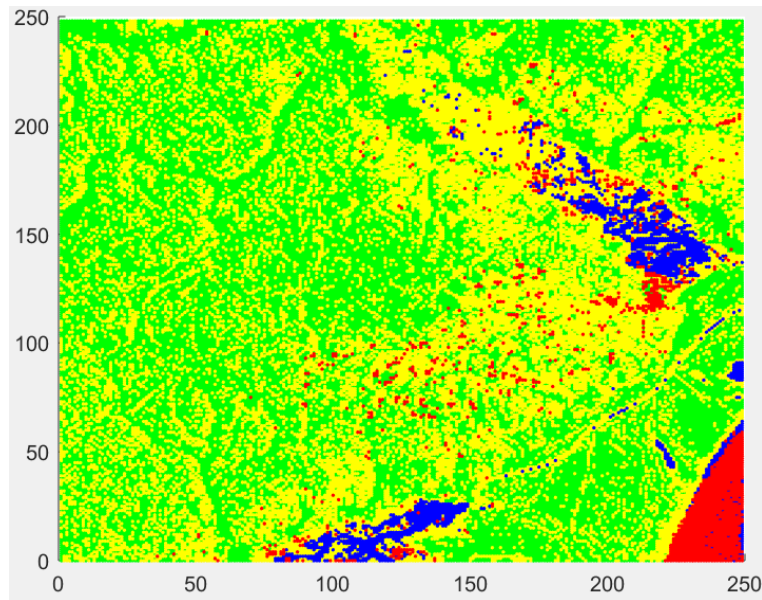


Figure 5.7: Four class SVM with blue as water, green as forest, yellow farmland, and red urban

The above classification results were generated using the mean of each 3x3 window in the Freeman and Durden calculation. That is, the mean of each complex scattering component is computed over the window size, which in this case is nine pixels. This is also known as calculating the ensemble average over all of the pixels in the window and will represent the expectation of the scattering components in the Freeman and Durden equations. However, it is difficult to ensure that the mean of the nine pixel samples in the window represent the true expected value of the scattering components in that window. If outliers are present in the window, the mean could be drastically affected, resulting in a poor estimate of the expected value of the scattering matrix in the window. This will in turn throw off the calculations for the Freeman and Durden scattering mechanisms and affect the classification performance of the algorithm.

Alternatively, in figure 5.8, the median of the window scattering components is used in both the training of the SVM and the testing of the results. The median estimator was chosen since it is significantly less impacted by outliers in general. It should be noted that many more complex classes of estimators used for outlier suppression have also been proposed in the field of robust statistics. Huber introduced a class of so-called M-estimators specifically for the purpose of mitigating the effect of outliers [18]. Maximum likelihood estimation is one such M-estimator. In the median estimator case explored here, there seems to be a slight increase in performance using the median in place of the mean. In particular, the water areas denoted with blue dots appear more crisp and less diluted with the false urban (red) classification. Figure 5.8 shows the median performing better in classifying the river in the lower right corner as water versus using the mean estimator in figure 5.7.

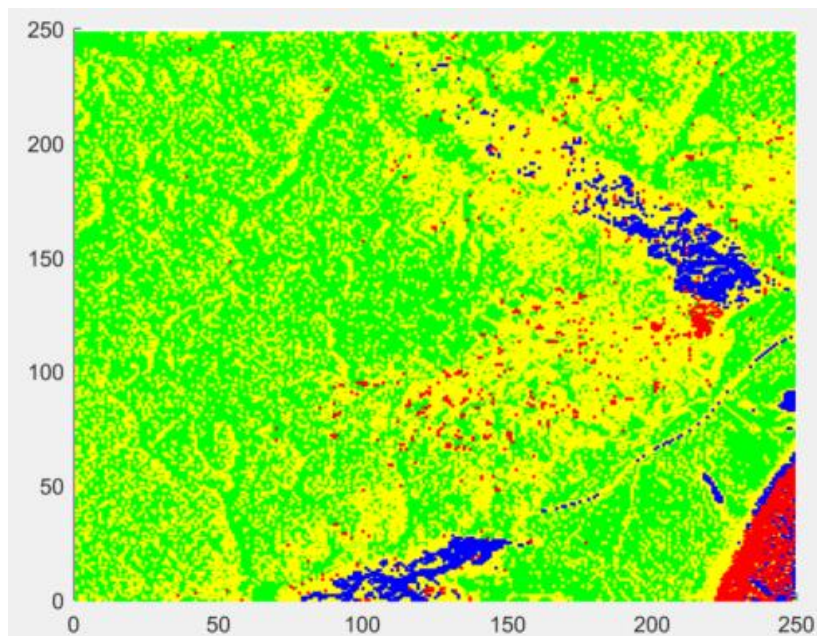


Figure 5.8: Four class results using the median estimator

In order to quantify the results for the different number of classes chosen in the SVM model, the total number of pixels assigned to each class for each SVM model is shown in Table 5.1. The sample average estimator was used for all the models in the table for accurate comparison. It would be best to have this compared to the number of pixels that are actually in each class according to the ground truth. However, the accuracy of the ground truth is not good enough for such a comparison. Note that the water percentage slowly decreases as the number of classes in the model is increased and the ability to accurately discriminate water decreases. The 5.0% from the 2-class model is likely the most accurate just looking at the crispness of the resulting image compared to the SAR image.

	Forest	Farm	Water	Urban
2-Class SVM	N/A	58926 (95.0%)	3075 (5.0%)	N/A
3-Class SVM	33615 (54.2%)	26516 (43.8%)	1870 (3.0%)	N/A
4 Class SVM	34320 (55.4%)	23929 (38.6%)	1797 (2.9%)	1955 (3.2%)

Table 5.1 Classification Results by Pixel Percentage for all SVM Models

The previous classification results were used to test the ability of model to discriminate between major land types such as urban area and forest. However, more specific subtypes such as different kinds of forest were not included in the classes. This is an important subject of the study because a goal is to use this classification model to characterize the regrowth stages of rainforest environments to determine the health of the forest and any deforestation. In order to simplify the model and due to the availability of truth data, only two forest types were

distinguished. The first type is secondary vegetation and includes lower canopy areas in an intermediate forest growth stage. The other class was primary forest which is characterized by higher and more dense canopies than secondary vegetation.

For the training data in the SVM model, more training areas were used than the previous results. Specifically, each class had two separate training areas verses the one training area in the previous terrain results. The goal of this was to account for slight differences between areas that should be labeled as the same class to make the model more robust. In figure 5.9, the red squares highlight the secondary vegetation training areas and the blue are the primary forest training areas.

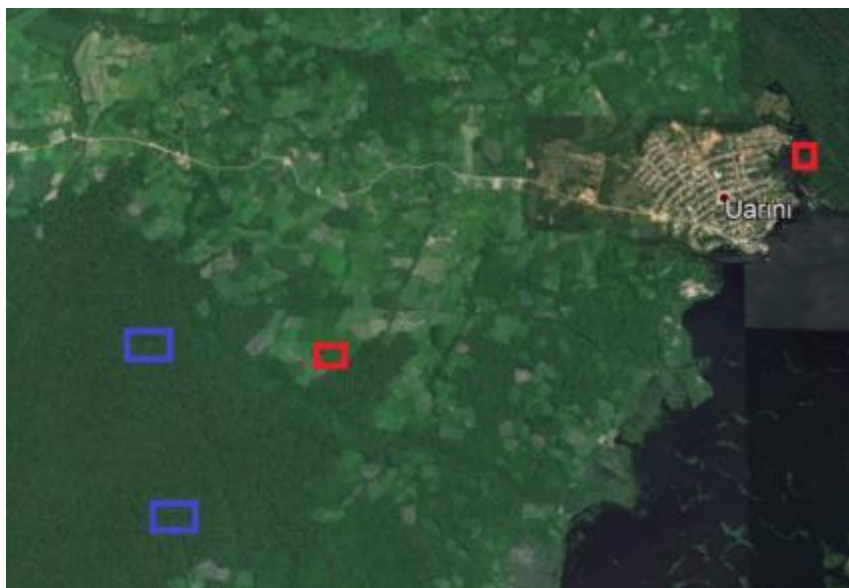


Figure 5.9: Training data areas for the forest discrimination.

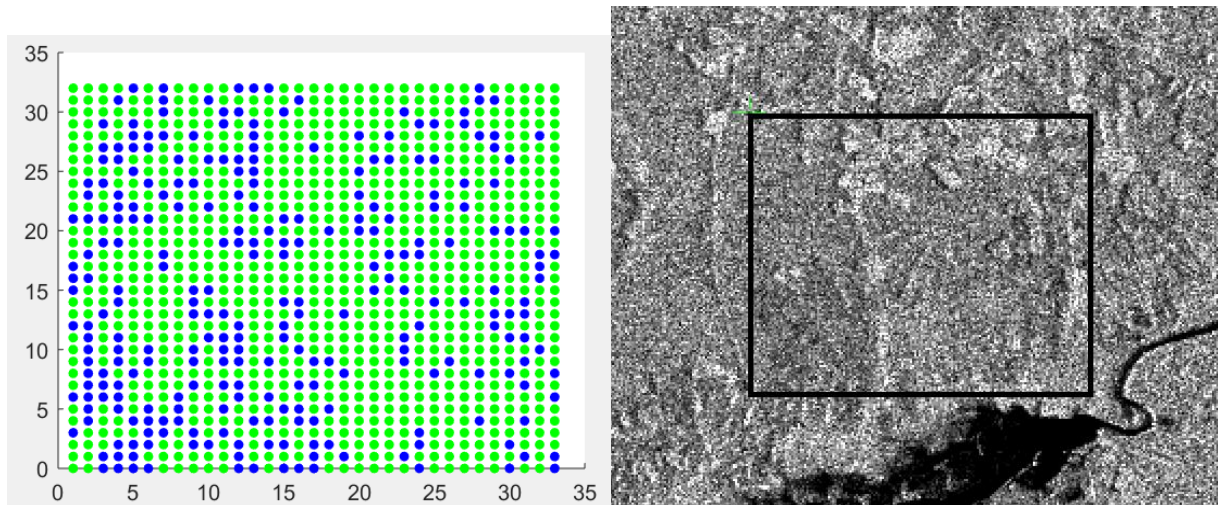


Figure 5.10: Classification results (left) of raw SAR image (right) for two forest classes. Green is primary forest and blue is secondary forest.

The results of the two classes of forest types in figure 5.10 appears to have significant misclassifications. The areas that should be secondary forest are not clearly defined in the classification results. However, overall the sample image was mostly classified as primary forest which probably 80-90% of the sample area actually is. It is likely that with more separate training areas of each type, the classification results could be improved.

Chapter 6

Conclusions and Future Work

6.1) Conclusions

In this work, the Freeman and Durden scattering model was applied to fully polarimetric SAR data and a support vector machine classification method was used to discriminate class types in a tropical rainforest environment. An efficient method for solving the Freeman and Durden complex system of equations was developed and implemented in Matlab. Solving the system directly proved to be significantly faster than both Newton's method and the gradient descent method (Appendix A). Next, the classification capability of the model was put to the test specifically on the Amazon rainforest land cover types. For the two-class case, the trained SVM model worked very well with very few misclassifications. As the model was implemented on more class types, however, the performance of the model decreased substantially. For example, much of the largest body of water in the test image was misclassified as the urban land cover type. Perhaps this was due to insufficient quality or quantity of training data for those two land

cover types. Interestingly, in the three-class case, the same portion of water in the test image was misclassified as farmland. Even in the two-class case, there were misclassifications as well in that area. This is unexpected since water areas in a SAR image should be easily distinguishable from the rest of the land areas. Calm water should have a uniform signature very different from complex multi-bounce in urban environments and canopy/volume scatter in forest environments. However, if the water in that area had a rougher state, perhaps double bounce scatter is more pronounced due to the waves. Therefore, that water was being classified as “urban” which is typically dominated by double bounce man-made structures.

Employing the median to the multi-pixel windowing helped alleviate the misclassification problem in the large water area. It should be noted that the median estimator was used for both the training data and the classification results in figure 5.8. It is likely that the use of the median on the training data was more beneficial than using the median in the classification step. The training data used for each class was a small area which would have been greatly affected by outliers if the average was used instead of the median. The median should have helped smooth out the effects of any outliers in the training data.

6.2) Future Work

This research only considered the Freeman-Durden scattering model to generate the features used for classification. While this model includes the three major polarimetric radar scattering mechanisms, the Yamaguchi model adds a fourth helical mechanism which may more accurately describe the backscatter physics. Future work could replace the Freeman and Durden model with the Yamaguchi model in the feature extraction step and compare the results. Support

Vector Machine methods are known to perform well in relatively high dimensional feature spaces, so the addition of the helical scattering feature may improve the overall classification performance.

Other features could also be added to see if they improve the overall classification performance of the SVM model. Alpha-Entropy is a well know decomposition technique that would add two useful features to the feature space. Additionally, SAR collection parameters could possibly be added to the feature space. For example, many scattering effects are dependent on the grazing angle of the collection. For a space-based collection system, the grazing angle will change significantly on orbit passes of a ground region. If grazing angle were added as a feature to the model, it may help with classification performance if enough training data was ingested at representative grazing angles.

In this research, a simple, though effective, approach was taken to train the model. For each class, only one small region was used as the training data for the SVM classifier. That trained classifier was then used on the rest of the much larger image. In order to build a more robust classifier, the training data for each class should be increased substantially and taken from multiple regions of the image for each class. Preferably, the training data should also be taken from multiple images for each class as well.

Support Vector Machine was the only supervised learning technique that was employed in the method and simulation results in this study. SVM was chosen for computational simplicity and proven ability to perform well in higher dimension feature spaces. Other methods such as the maximum likelihood classifier using the Wishart distribution and deep neural networks are proven machine learning techniques. It would be useful to implement these

techniques with the Freeman and Durden model and compare the classification results to Support Vector Machine.

While the L-band SAR imagery from ALOS PALSAR that was used to test the SVM model has been shown to be effective in vegetation classification problems, other frequency bands of SAR data could be explored as well. For example, RADARSAT-2 is a fully polarimetric SAR sensor platform that operates in C-band. The C-band data from RADARSAT-2 has been used too in classification applications such as crop identification, forestry classification, and ice cap studies. TerraSAR-X is another polarimetric SAR satellite-based platform that operates at the X-band frequency and the dataset has been shown to provide better final classification accuracies than C-band datasets by about 10 percent [19]. It would be useful in future work to compare the classification capability of the model using different bands of input polarimetric SAR data and determine the optimal band for each application.

Finally, future work should involve new applications for using the classification techniques developed in this research. In this work, the classification application was focused on land cover types in the Amazon rainforest specifically for purposes of tracking deforestation and forest regrowth. There is always an ideal classification technique for every application and it is not always obvious which technique will work well with which application. Therefore, it would be prudent to test the classification methods on multiple applications and determine which applications work best. Some classification applications that could be explored with fully polarimetric SAR data are crop identification, hydrology, polar ice studies, and geology.

References

- [1] Negri R., Dutra L., Freitas C., and Lu D., “Exploring the Capability of ALOS PALSAR L-Band Fully Polarimetric Data for Land Cover Classification in Tropical Environments,” *IEEE Journal of Selected Topics in Applied Earth Observations and Remote Sensing*, 2016.
- [2] Hughes G., “On the Mean Accuracy of Statistical Pattern Recognizers,” *IEEE Transactions on Information Theory*, 1968.
- [3] Cloude S. and Pottier E., “An Entropy Based Classification Scheme for Land Applications of Polarimetric SAR,” *IEEE Transactions on Geoscience and Remote Sensing*, 1997.
- [4] Freeman A. and Durden S., “A Three-Component Scattering Model for Polarimetric SAR Data,” *IEEE Transactions on Geoscience and Remote Sensing*, 1998.
- [5] Richards M., *Fundamentals of Radar Signal Processing*, Second Edition. McGraw-Hill Education, 2014.
- [6] Yamaguchi Y., Yajima Y., and Yamada H., “A Four-Component Decomposition of POLSAR Images Based on the Coherency Matrix,” *IEEE Geoscience and Remote Sensing Letters*, 2006.

- [7] Li G., Lu D., Moran E., and Dutra L. V., and Batistella M., “A comparative analysis of ALOS PALSAR L-band and radarsat-2 C-band data for land cover classification in a tropical moist region,” *ISPRS J. Photogramm. Remote Sens.*, vol. 70, pp. 26–38, 2012.
- [8] Duda R., Hart P., and Stork D., *Pattern Classification*, Second Edition, John Wiley and Sons, U.K. 2006.
- [9] Cortes C. and Vapnik V., “Support-Vector Networks,” AT&T Labs-Research, 1995.
- [10] Chen K., *Principles of Synthetic Aperture Radar Imaging - A System Simulation Approach*, Taylor and Francis Group, Florida, 2016.
- [11] Cloude, S. R., “Polarisation: Applications in Remote Sensing”, Oxford University Press, Oxford, 2009.
- [12] Carrara W., Goodman R., and Majewski R., *Spotlight Synthetic Aperture Radar Signal Processing Algorithms*, Artech House, 1995.
- [13] Adams J., Rowlandson T., Mckeown S., Berg A., McNairn H., and Sweeney S., “Evaluating the Cloude-Pottier and Freeman-Durden scattering decompositions for distinguishing between unharvested and post-harvest agricultural fields,” *Canadian Journal of Remote Sensing*, 2013.

- [14] Mascolo L., Vicente-Guijalba F., and Migliaccio M., “A Complete Procedure for Crop Phenology Estimation with PolSAR Data Based on the Complex Wishart Classifier,” *IEEE Transactions on Geoscience and Remote Sensing*, 2016.
- [15] Lee J., Grunes M., Ainsworth T., Du L., Schuler D., and Cloude S., “Unsupervised Classification Using Polarimetric Decomposition and the Complex Wishart Classifier,” *IEEE Transactions on Geoscience and Remote Sensing*, 1999.
- [16] Anfinson S., Jenssen R., and Eltoft T., “Spectral Clustering of Polarimetric SAR Data with Wishart-Derived Distance Measures,” University of Tromso, Norway.
- [17] Maghsoudi Y., Collins M., and Leckie D., “RadarSat-2 Polarimetric SAR Data for Boreal Forest Classification Using SVM and a Wrapper Feature Selector,” *IEEE Journal of Selected Topics in Applied Earth Observations and Remote Sensing*, 2013.
- [18] Huber P. J., *Robust Statistics*, New York: Wiley, 1981.
- [19] McNairn H., Shang J., Champagne C., and Jiao X., “TerraSAR-X and RADARSAT-2 for Crop Classification and Acreage Estimation,” *IEEE International Geoscience and Remote Sensing Symposium*, 2009.

Appendix A

Implementation of Proposed Model in Matlab

Function to solve Freeman-Durden equations (Newton's method commented) with median windowing estimation:

```
%This function reads in the amplitude and phase pixel info and creates matrices for each of
%the three scattering powers (volume, surface, and double bounce)
%the arguments define a window on which the scattering powers are
%decomposed

function [Ps_med, Pv_med, Pd_med] = Freeman_durden_function(x1,x2,y1,y2,k,m,Ls,Ss)

%Read in the amplitude and phase data for each polarization
SHH_A = imread('ALPSRP254257130-P1.1__A_AMP-HH.tif','PixelRegion',{[Ls+3*(k-1)+1,Ls+3*k],[Ss+3*(m-1)+1,Ss+3*m]});
SHH_P = imread('ALPSRP254257130-P1.1__A_PHASE-HH.tif','PixelRegion',{[Ls+3*(k-1)+1,Ls+3*k],[Ss+3*(m-1)+1,Ss+3*m]});
SVV_A = imread('ALPSRP254257130-P1.1__A_AMP-VV.tif','PixelRegion',{[Ls+3*(k-1)+1,Ls+3*k],[Ss+3*(m-1)+1,Ss+3*m]});
SVV_P = imread('ALPSRP254257130-P1.1__A_PHASE-VV.tif','PixelRegion',{[Ls+3*(k-1)+1,Ls+3*k],[Ss+3*(m-1)+1,Ss+3*m]});
SHV_A = imread('ALPSRP254257130-P1.1__A_AMP-HV.tif','PixelRegion',{[Ls+3*(k-1)+1,Ls+3*k],[Ss+3*(m-1)+1,Ss+3*m]});
SHV_P = imread('ALPSRP254257130-P1.1__A_PHASE-HV.tif','PixelRegion',{[Ls+3*(k-1)+1,Ls+3*k],[Ss+3*(m-1)+1,Ss+3*m]});

%Convert data to double format
SHH_A = double(SHH_A);
SHH_P = double(SHH_P);
SVV_A = double(SVV_A);
SVV_P = double(SVV_P);
SHV_A = double(SHV_A);
SHV_P = double(SHV_P);

%find middle of window value
x3=2;
y3=2;

%Convert data to complex numbers
SHH_real = SHH_A*cos(pi/180*SHH_P);
SHH_comp = SHH_A*sin(pi/180*SHH_P);
SVV_real = SVV_A*cos(pi/180*SVV_P);
SVV_comp = SVV_A*sin(pi/180*SVV_P);
SHV_real = SHV_A*cos(pi/180*SHV_P);
SHV_comp = SHV_A*sin(pi/180*SHV_P);

SHH = SHH_real + SHH_comp*j;
SVV = SVV_real + SVV_comp*j;
SHV = SHV_real + SHV_comp*j;
```

```

%median (or change to mean() for these 4 lines)
SHH1=median(median((abs(SHH)).^2));
SHV1=median(median((abs(SHV)).^2));
SVV1=median(median((abs(SVV)).^2));
SHH_SVV=median(median(SHH*conj(SVV)));

%calculate fv
fv=3*SHV1;

%If real(SHH*conj(SVV)) is positive, then surface scatter is dominant:
if real(SHH_SVV) > 0

    a=-1;

% Implement Newton's method
% x0=[10^12 10^12 1]'; % seem to be the right initial conditions
% x0=[10^12 10^12 1]';
% fs=x0(1);
% fd=x0(2);
% B=x0(3);
% f=[fs*(abs(B))^2+fd*(abs(a))^2-SHH1;fs+fd-SVV1;fs*B+fd*a-SHH_SVV];
% J=[(abs(B))^2 2*fs; 1 1 0; B -1 fs];
% J_inv=1/(B^2*fs-fs+2*fs*(-1-B))*[fs -fs -1-B;-3*fs fs*B^2-2*fs*B B^2+B;-2*fs 2*fs B^2-1]';
% for i=1:1
% dx=-J\f
% x0=x0+dx;
% x0=x0-J_inv*f; %Newton's method
% x0=x0-10^-24*ctranspose(J)*f % Gradient descent
% x0=x0-1e-25*(ctranspose(J)*f+ctranspose(J)*conj(f))
% fs=x0(1);
% fd=x0(2);
% B=x0(3);
% f=[fs*(abs(B))^2+fd*(abs(a))^2-SHH1;fs+fd-SVV1;fs*B+fd*a-SHH_SVV];
% J=[(abs(B))^2 2*fs; 1 1 0; B -1 fs];
% J_inv=1/(B^2*fs-fs+2*fs*(-1-B))*[fs -fs -1-B;-3*fs fs*B^2-2*fs*B B^2+B;-2*fs 2*fs B^2-1]';
% end
% Ps = abs(double(fs*(1+(abs(B)^2))));
% Pd = abs(double(fd*(1+(abs(a)^2))));
% Pv = abs(8*fv/3);
% end Newtons

%START analytic solution
%apply quadratic formula to find B
%plus solution
B=(-(SVV1*(abs(a))^2-SHH1)+sqrt((SVV1*(abs(a))^2-SHH1)^2-4*(SHH_SVV-SVV1*a)*(-SHH_SVV*(abs(a))^2+SHH1*a)))/(2*(SHH_SVV-SVV1*a));
%minus solution
%B=(-(SVV1*(abs(a))^2-SHH1)-sqrt((SVV1*(abs(a))^2-SHH1)^2-4*(SHH_SVV-SVV1*a)*(-SHH_SVV*(abs(a))^2+SHH1*a)))/(2*(SHH_SVV-SVV1*a));
fs=(SHH_SVV-SVV1*a)/(B-a);
fd=SVV1-fs;
Ps = abs(double(fs*(1+(abs(B)^2))));
Pd = abs(double(fd*(1+(abs(a)^2))));

```

```

Pv = abs(8*fV/3);
%End analytic solution
else
%If real(SHH*conj(SVV)) is negative, then double bounce is dominant:
B=1;

%Implement Newton's method
% x0=[10^12 10^12 1]'; % seem to be the right initial conditions
% x0=[10^12 10^12 1]';
% fs=x0(1);
% fd=x0(2);
% a=x0(3);
% f=[fs*(abs(B))^2+fd*(abs(a))^2-SHH1;fs+fd-SVV1;fs*B+fd*a-SHH_SVV];
% J=[1 (abs(a))^2 2*fd; 1 1 0; 1 a fd];
% J_inv=1/(fd-fd*(abs(a))^2+2*fd*(a-1))*[fd -fd a-1;fd*(abs(a))^2-2*a*fd -fd -a+(abs(a))^2;-2*fd 2*fd 1-
(abs(a))^2]';
% for i=1:3
% % dx=-J*f;
% % x0=x0+dx;
% x0=x0-J_inv*f; % Newton's method
% % x0=x0-10^-30*J'*f % Gradient descent
% fs=x0(1);
% fd=x0(2);
% a=x0(3);
% f=[fs*(abs(B))^2+fd*(abs(a))^2-SHH1;fs+fd-SVV1;fs*B+fd*a-SHH_SVV];
% J=[1 (abs(a))^2 2*fd; 1 1 0; 1 a fd];
% J_inv=1/(fd-fd*(abs(a))^2+2*fd*(a-1))*[fd -fd a-1;(abs(a))^2*fd-2*a*fd -fd -a+(abs(a))^2;-2*fd 2*fd 1-
(abs(a))^2]';
% end
% Ps = abs(double(fs*(1+(abs(B)^2))));
% Pd = abs(double(fd*(1+(abs(a)^2))));
% Pv = abs(8*fV/3);
%end Newtons

%Start analytic solution
%apply quadratic formula to find a
Ca=SVV1*B-SHH_SVV;
Cb=-SVV1*(abs(B))^2+SHH1;
Cc=SHH_SVV*(abs(B))^2-SHH1*B;
%plus solution
a=(-Cb+sqrt(Cb^2-4*Ca*Cc))/(2*Ca);
%minus solution
%a=(-Cb-sqrt(Cb^2-4*Ca*Cc))/(2*Ca);
fs=(SHH_SVV-SVV1*a)/(B-a);
fd=SVV1-fs;
Ps = abs(double(fs*(1+(abs(B)^2))));
Pd = abs(double(fd*(1+(abs(a)^2))));
Pv = abs(8*fV/3);
%end solve equations analytically
end

%output the median values for each scattering power
Ps_med=median(median(Ps));
Pv_med=median(median(Pv));

```

```

Pd_med=median(median(Pd));

end

```

Computing the Scattering Components of an Image Window:

```

%This script calculates the freeman-durden composition (using the freeman-durden function) for a given sample
%of a image and window size, and plots the three scattering powers over the
%sample image
%define line and sample region
tic

% test region
L1=783;
L2=1530;
S1=416;
S2=1163;

%set line and sample to the image evaluation limits

x1=L1;
x2=L2;
y1=S1;
y2=S2;

%calculate the number of samples using a 3x3 window
rx=(L2-L1)/3;
ry=(S2-S1)/3;;

%calculate the Freeman_durden decomposition on each window and store
%scattering powers a matrix
for i=1:rx
    for j=1:ry

        [Ps1, Pv1, Pd1] = Freeman_durden_function_3x3_v2(L1+(i-1)*3,L1+i*3,S1+(j-1)*3,S1+j*3,i,j,L1,S1);
        Ps_mat(i,j)=Ps1;
        Pv_mat(i,j)=Pv1;
        Pd_mat(i,j)=Pd1;

    end
end
toc

```

Support Vector Machine Classifier:

```

%This script imports freeman-durden power data as training matrices for an
%SVM model. It then uses test data to predict classes using the trained
%SVM model. This script works for 4 classes so far. It plots the
%classification results for the test data.
tic
%define test image size
Length=83;
Width=83;

```

```

%Define urban area training matrices (log10 of the original)
Ps_urban = [ 12.9046 12.8348 12.6520 12.8015 12.4603;
 12.7582 12.9269 13.1831 13.1016 12.6513;
 13.1073 12.8745 12.9371 12.9091 12.5998;
 12.4188 12.8326 12.9443 12.6317 12.7837;
 12.1924 12.8502 12.7442 12.5910 12.4041];

Pv_urban = [ 12.1546 11.8951 12.0218 12.0179 11.8208;
 11.8294 11.9208 11.9748 12.0875 11.9017;
 12.1966 12.0113 11.7236 11.9821 12.0738;
 11.7983 11.8556 11.7820 11.9026 11.8237;
 11.8773 11.8162 11.7102 11.8835 11.8291];

Pd_urban = [ 12.5608 12.4744 12.3095 12.4190 12.1326;
 12.4349 12.5915 12.8741 12.7743 12.3663;
 12.8464 12.6050 12.6408 12.5484 12.2816;
 12.1487 12.5945 12.5958 12.3137 12.4476;
 11.8874 12.5751 12.3986 12.2616 12.0381];

Ps_urban_row = [Ps_urban(:,1)' Ps_urban(:,2)' Ps_urban(:,3)' Ps_urban(:,4)' Ps_urban(:,5)'];
Pv_urban_row = [Pv_urban(:,1)' Pv_urban(:,2)' Pv_urban(:,3)' Pv_urban(:,4)' Pv_urban(:,5)'];
Pd_urban_row = [Pd_urban(:,1)' Pd_urban(:,2)' Pd_urban(:,3)' Pd_urban(:,4)' Pd_urban(:,5)'];

Pd_urban_pred = [Ps_urban_row; Pv_urban_row; Pd_urban_row]';

%Define water area training matrices (log10 of the original)
Ps_water = [ 11.1243 10.8993 10.9027 10.8358 11.0104;
 11.0188 11.0764 10.9367 10.9501 10.9730;
 11.0188 10.9518 10.9807 10.9714 11.0038;
 10.8739 10.8980 10.9205 10.9327 10.9726;
 10.9158 10.9220 10.9313 10.9092 10.8921];

Pv_water = [11.0694 10.9366 10.8751 10.9543 11.0079;
 10.8103 10.8347 10.6947 10.9168 11.0167;
 10.8373 10.8523 10.7674 10.8034 11.0039;
 10.8093 10.6739 10.8041 10.8148 10.7984;
 10.7722 10.8566 10.8467 10.7581 10.8143];

Pd_water = [10.8194 10.5983 10.6219 10.5401 10.7199;
 10.7106 10.7317 10.6441 10.6295 10.6804;
 10.7225 10.6726 10.6887 10.6712 10.6916;
 10.5772 10.5944 10.5974 10.6191 10.6569;
 10.6030 10.6201 10.6366 10.5703 10.5657];

Ps_water_row = [Ps_water(:,1)' Ps_water(:,2)' Ps_water(:,3)' Ps_water(:,4)' Ps_water(:,5)'];
Pv_water_row = [Pv_water(:,1)' Pv_water(:,2)' Pv_water(:,3)' Pv_water(:,4)' Pv_water(:,5)'];
Pd_water_row = [Pd_water(:,1)' Pd_water(:,2)' Pd_water(:,3)' Pd_water(:,4)' Pd_water(:,5)'];

Pd_water_pred = [Ps_water_row; Pv_water_row; Pd_water_row]';

%Define farm area training matrices (log10 of the original)
Ps_farm = [12.5503 12.1432 12.4499 12.3177 12.4626;
 12.2150 12.2803 12.2168 12.4165 12.4670;
 12.5078 12.2784 12.3691 12.3054 12.4110;
 12.5024 12.4910 12.3791 12.1808 12.1506;

```

```

12.3854 12.3874 12.3402 12.0808 12.3295];

Pv_farm = [12.2411 12.0464 12.4356 12.3202 12.2793;
12.0072 12.1312 12.0233 12.3351 12.2390;
12.0660 12.1793 12.0101 12.1941 12.2702;
12.2805 12.3103 12.2323 11.7675 11.9552;
12.1256 12.3815 12.1361 11.9425 12.2244];

Pd_farm = [12.2361 11.8433 12.1510 12.0188 12.1602;
11.9455 12.0024 11.9201 12.1220 12.1592;
12.1846 11.9858 12.0747 11.9871 12.1251;
12.1898 12.1891 12.0629 11.8889 11.8354;
12.1160 12.0867 12.0205 11.7717 12.0314];

Ps_farm_row = [Ps_farm(:,1)' Ps_farm(:,2)' Ps_farm(:,3)' Ps_farm(:,4)' Ps_farm(:,5)'];
Pv_farm_row = [Pv_farm(:,1)' Pv_farm(:,2)' Pv_farm(:,3)' Pv_farm(:,4)' Pv_farm(:,5)'];
Pd_farm_row = [Pd_farm(:,1)' Pd_farm(:,2)' Pd_farm(:,3)' Pd_farm(:,4)' Pd_farm(:,5)'];

Pd_farm_pred = [Ps_farm_row; Pv_farm_row; Pd_farm_row]';

%Define forest area training matrices (log10 of the original)

Ps_forest = [12.3246 12.3372 12.3772 12.4643 12.5337;
12.3543 12.2369 12.3119 12.3964 12.4120;
12.4656 12.3145 12.3361 12.3102 12.4525;
12.4478 12.3352 12.3576 12.2805 12.3173;
12.3085 12.1832 12.3821 12.3545 12.3791];

Pv_forest = [12.1816 12.2443 12.1566 12.2340 12.3100;
12.2344 12.0534 12.1258 12.3344 12.3101;
12.1540 12.2121 12.1536 12.1890 12.2880;
12.2616 12.1940 12.1386 12.0213 12.1146;
12.0445 12.1073 12.1065 12.2027 12.2794];

Pd_forest = [12.0320 12.0401 12.0683 12.1712 12.2209;
12.0625 11.9383 11.9905 12.0892 12.1323;
12.1535 12.0126 12.0181 11.9865 12.1637;
12.1412 12.0601 12.0412 12.0092 12.0292;
12.0042 11.8918 12.0788 12.0617 12.0940];

Ps_forest_row = [Ps_forest(:,1)' Ps_forest(:,2)' Ps_forest(:,3)' Ps_forest(:,4)' Ps_forest(:,5)'];
Pv_forest_row = [Pv_forest(:,1)' Pv_forest(:,2)' Pv_forest(:,3)' Pv_forest(:,4)' Pv_forest(:,5)'];
Pd_forest_row = [Pd_forest(:,1)' Pd_forest(:,2)' Pd_forest(:,3)' Pd_forest(:,4)' Pd_forest(:,5)'];

Pd_forest_pred = [Ps_forest_row; Pv_forest_row; Pd_forest_row]';

%combine the four matrices

Pred_mat = ([Pd_forest_pred; Pd_farm_pred; Pd_water_pred; Pd_urban_pred]);

%create the class labels (-1 is forest, 1 is farm, 2 is water, 3 is urban)
theclass = ones(100,1);
theclass(1:25) = -1;
theclass(51:75) = 2;

```

```

theclass(76:100) = 3;

%create the model
%for multiclass use fitcecoc

%SVMModel = fitsvm(Pred_mat,theclass,'KernelFunction','linear',...
    %'BoxConstraint',Inf,'ClassNames',[-1,1]);
SVMModel = fitcecoc(Pred_mat,theclass);

%perform cross validation to test model accuracy
cross_val = crossval(SVMModel);
misclass1 = kfoldLoss(cross_val);
misclass1

%Define test matrix
Ps_test = log10(Ps_mat);

Pv_test = log10(Pv_mat);

Pd_test = log10(Pd_mat);

Ps_test_row = reshape(Ps_test,[1,62001]);
Pv_test_row = reshape(Pv_test,[1,62001]);
Pd_test_row = reshape(Pd_test,[1,62001]);

Pd_test_pred = ([Ps_test_row; Pv_test_row; Pd_test_row]);

%do the prediction based on the SVM model
[label,score] = predict(SVMModel,Pd_test_pred);

label_new = reshape(label,[249,249]);

%build the data and then the scatterplot

%green for forest
[green_loc_row, green_loc_col] = find(label_new==-1);

%yellow for farm
[yellow_loc_row, yellow_loc_col] = find(label_new==1);

%blue for water
[blue_loc_row, blue_loc_col] = find(label_new==2);

%red for urban
[red_loc_row, red_loc_col] = find(label_new==3);

%set the maker size
sz=3;

scatter(green_loc_col, 249 - green_loc_row,sz,'g','filled');
hold on
scatter(yellow_loc_col, 249 - yellow_loc_row,sz,'y','filled');
hold on
scatter(blue_loc_col, 249 - blue_loc_row,sz,'b','filled');
hold on

```

```
scatter(red_loc_col, 249 - red_loc_row, sz, 'r', 'filled');
```

```
toc
```